Author/s:
MacArthur, KE;D'Alfonso, AJ;Ozkaya, D;Allen, LJ;Nellist, PD

Title:
Optimal ADF STEM imaging parameters for tilt-robust image quantification

Date:
2015-09-01

Citation:
MacArthur, K. E., D'Alfonso, A. J., Ozkaya, D., Allen, L. J. & Nellist, P. D. (2015). Optimal ADF STEM imaging parameters for tilt-robust image quantification. Ultramicroscopy, 156, pp.1-8. https://doi.org/10.1016/j.ultramic.2015.04.010.

Persistent Link:
https://hdl.handle.net/11343/217344

Optimal ADF STEM imaging parameters for tilt-robust image quantification

K.E. MacArthur[1], A.J. D'Alfonso[2], D. Ozkaya[3], L.J. Allen[2], P.D. Nellist[1]

1: Department of Materials, University of Oxford, Parks Road, OX1 3PH, UK

2: School of Physics, University of Melbourne, Parkville Victoria 2010, Australia

3: Johnson Matthey Technology Centre, Blounts Court Road, Sonning Common, Reading, RG4 9NH, UK

Email: katherine.macarthur@materials.ox.ac.uk

Address: Department of Materials, 13 Parks Road, Oxford, UK, OX13PH

Telephone: +44(0) 1865 273657

Abstract

An approach towards experiment design and optimisation is proposed for achieving improved accuracy of ADF STEM quantification. In particular, improved robustness to small sample mis-tilts can be achieved by optimising detector collection and probe convergence angles. A decrease in cross section is seen for tilted samples due to the reduction in channelling, resulting in a quantification error, if this is not taken into account. At a smaller detector collection angle the increased contribution from elastic scattering, which initially increases with tilt, can be used to offset the decrease in the TDS signal.

Keywords: quantitative ADF, electron channelling, sample tilt

1 – Introduction

Atomic-resolution annular dark-field scanning transmission electron microscopy (ADF STEM) is a powerful tool for materials characterisation due to the ease of interpretability of the images. Collecting the scattered electrons through a large range of angles using an annular shaped detector yields an incoherent image, also referred to as Z-contrast image, with both thickness and compositional information [1]. This provides valuable qualitative information about material structures at the atomic scale.

ADF STEM quantification treats these images as numerical datasets for either comparison with careful simulation or statistical interpretation methods to reveal more information about material structures [2–7]. Early attempts to quantify particle size and therefore size-distributions of small metallic nanoparticles [8,9] assumed that the total intensity of the particles scaled linearly with the number of atoms they contain. This, however, ignores any channelling effects when imaging crystals, particularly along a low order zone-axis. More recently quantitative STEM has turned towards recording the ADF images on a calibrated intensity scale with each pixel in the image having a value given by the number of electrons scattered out to the detector expressed as a fraction of the number of electrons in the incident probe [10]; and accounting for any asymmetries in the detector hardware [11,12]. These normalised images can be used to extract atom counts or composition by comparing directly with simulations [3,13].

An alternative to the comparison with simulations is a statistical method pioneered by Van Aert et al. [14,15]. The statistical approach, which is not dependent on normalised experimental image intensities, relies on decomposing the distribution of integrated intensities or 2-dimensional volumes into a sum of Gaussian components, which can then be related back to atom counts. In this way it can be used to provide an independent measure of atom counts and is therefore

unaffected by errors in measuring imaging parameters. There is, however, a minimum requirement on number of observations per component, necessary for accurate determination of the number of components present within the image [16], which can pose a problem for imaging nanoparticles.

Comparison of calibrated image intensities with simulation, on a pixel by pixel basis, has previously relied on knowledge of a significant number of imaging parameters [17]. Many of these are time consuming to determine, risking beam damage, and may require changing samples. Here we make use of the cross section approach, first proposed by Retsky [18], which is mathematically identical to the 2-dimensional Gaussian volumes used by van Aert et al. [15] and is a valuable tool for ADF STEM quantification due to the robustness to a wide range of these imaging parameters including defocus, source size effects and coherence, and aberrations such as astigmatism [19]. This gives greater flexibility when imaging more challenging and beam sensitive samples where it may not be possible to know the microscope settings as accurately.

For direct interpretation of images and accurate quantification, on a column by column basis, cleanly resolved atomic resolution images are required; necessitating alignment of the sample down a low order zone axis [20]. When atoms are aligned in this way, parallel to the incident electron probe, they provide a small lensing and therefore focusing effect on the beam [21]. The subsequent atoms in the atomic column then experience a more focused probe than the first atom and so on; resulting in scattering to the detector that initially increases faster than linearly with respect to the number of atoms. Therefore the contribution of the second atom in a column to the total scattering cross section is larger than the contribution of the first, and so on. Along a longer column, oscillations in intensity are seen [22] and the process is often referred to as channelling. TDS simultaneously leads to a reduction in the electron intensity along a column which is often referred to as absorption. Channelling has considerable implications for ADF STEM. Heavier atoms

provide a stronger lensing effect than lighter atoms, which means that in columns containing a mixture of atom types the specific sequence of the atoms in the column will affect the resulting intensity scattered out to the detector [23].

In certain circumstances channelling can be exploited to expose subtle sample changes; for example it has been used advantageously to map the location of dopant atoms within an atomic column based on their contribution to the image intensity [24–27]. However, just as the additional scattering resulting from electron channelling must be considered when analysing quantitative ADF data, we must also be aware of the reduction in measured cross section when the sample is tilted away from a zone axis [19,20,28], and the atoms become less well aligned, which may result in an error in the comparison with simulation.

For more beam sensitive samples, such as catalyst nanoparticles, which are liable to rotate under the beam especially during sequential images [28], it is not usually possible to accurately tilt the sample to a low-order zone axis. Experimentally, smaller detector angles have been shown to demonstrate lower sensitivity to mis-tilt [28], which has been backed up by a statistical analysis of accuracy in atom assignments [29]. In this paper we show that it is possible to optimise the experimental parameters in order to minimise quantification errors should small sample mis-tilts occur. At low detector angles we find that the cross section is robust to limited tilts which we explain in terms of the balance between TDS (thermal diffuse scattering) and elastic scattering.

2 – Details of simulation

The study presented here is based on image simulations of an FCC Pt nanocube, viewed down the <110> crystallographic zone axis, 7 atoms in thickness. These image simulations also allow us to

investigate separately the behaviour of the elastic and TDS scattering, the importance of which will become apparent later. The simulations were carried out using the multislice quantum excitation of phonons (QEP) method [30] provided through the μSTEM software developed at the University of Melbourne [31] The software is optimized to provide fast parallel calculations on a graphical processing unit. All simulations presented use an accelerating voltage of 300kV and although they do not substantially affect the cross section calculation, a C_s of 4.06μm and C_5 of -1.25mm were also used, corresponding to the settings of a FEI Titan^3 instrument. The probe was focused on the entrance surface of the specimen. Unless otherwise stated detector angles of 35-190mrad and a probe convergence angle of 20.2mrad have been used.

All calculations were performed on a 0.98 x 1.25nm^2 nanocube containing 30 atomic columns, and 7 atoms (~1.94nm) in thickness in a 1.7 x 1.7 nm^2 super-cell, sampled on a 1024 x 1024 mesh. This results in a sampling equivalent to a maximum scattering angle of 376 mrad (approximately twice the outer detector angle), when bandwidth limiting is incorporated to prevent aliasing. The probe step size in the final output image is 0.01667nm. The thermal mean-square displacement of the atoms were calculated using the Gao and Peng parameterisation [32] and a temperature of 300K, which for Pt is 4.835×10^{-4} nm^2. An average was taken over 15 atomic configurations generated using these thermal displacement values. Source size was not included for the cross section calculations and has only been incorporated for the final published images when relating back to the predicted resolution for tilted images. The accepted method for an effective finite source size is to blur the images using a 2-dimensional Gaussian, here with a full width half maximum of 0.07nm [33]. Tilt was incorporated by rotating the coordinate system. The tilt angle was sufficiently small that no additional slicing was necessary. The sample was tilted towards the <001> direction away

from a <110> crystallographic zone axis. The same effect exists for other tilt axes or even an arbitrary tilt direction but for clarity only one is presented here [20].

Simulated images were used to calculate the scattering cross section of an atomic column as previously documented [19], by integrating over a Voronoi polygon. These values are represented in units of megabarn (Mb), which is $10^{-4}nm^2$.

Where stated the probe convergence angle and the inner detector angle have been systematically varied to assess their effect on the channelling contribution to the total cross section in order to determine experimental conditions for maximum robustness to sample tilts. The detector outer collection angle has been kept constant because it can often be governed by other factors than the value predicted from the inner-to-outer radius ratio of the hardware itself, such as physical apertures present in the post-specimen optics.

3 – The Tilt Dependence of Measured Cross Sections

Channelling of the electron probe provides additional scattered intensity over that predicted by assuming a linear multiplication of the cross section for 1 atom, as shown Figure 1. This additional scattering varies non-linearly with thickness making comparison with careful simulation essential for accurate quantification. At small sample thicknesses, below the first channelling length, the channelling contribution increases with thickness. Beyond this small oscillations are seen in the curve corresponding to the intensity oscillations down an atomic column. At the larger thicknesses the contribution from channelling begins to decrease again as absorption processes (mainly due to excitation of phonons, also known as thermal diffuse scattering) begin to dominate.

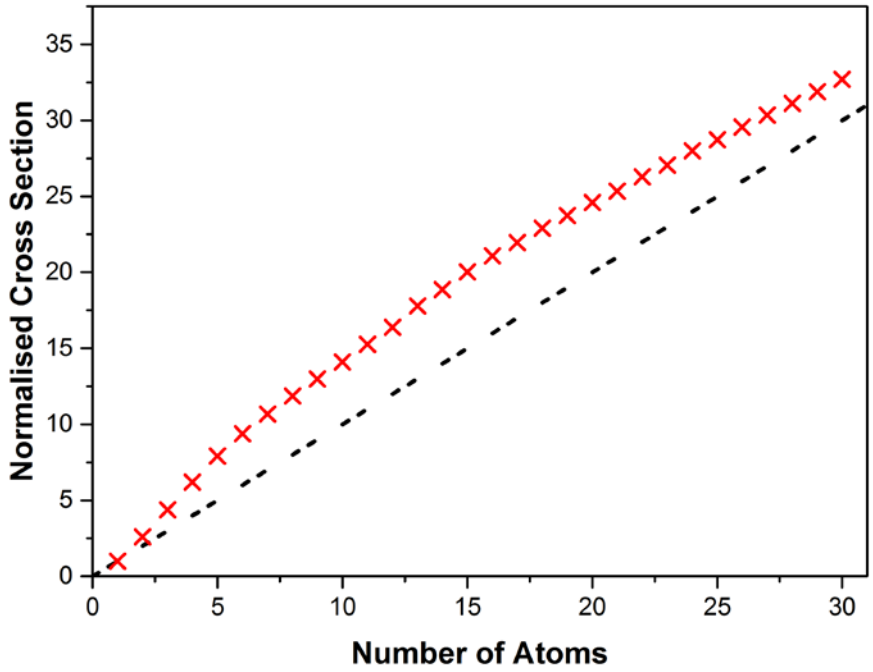

Figure 1 – Graph of cross section with increasing thickness of a single atomic-column of Pt normalised by the scattering from a single atom, for an inner detector angle of 35mrad. The dashed line has a gradient of one (linear model). The difference between the two lines is therefore the additional intensity provided by the atomic columns channeling the electron probe.

The additional intensity provided due to channelling is lost when a sample is tilted away from a low order zone axis and the atoms become less well aligned to the beam direction. In Figure 2 we evaluate the effect of detector collection angle, or camera length, on this reduction in cross section with sample tilt. As seen in Figure 2a there is a larger scattering cross section at smaller collection angles (such as 35mrad). This provides an improvement in signal per unit dose [34] as well as signal to noise gains, but could increase sensitivity to strain effects [35]. We also see a plateau begin to develop where the cross section is robust to small sample tilts. At the larger inner collection angles (such as 80mrad) the relative cross section drops off more rapidly with sample tilt (Figure 2b) which would provide a greater sensitivity to mis-tilt errors in quantification.

By separating out how the intensity varies across a series of concentric rings (Figure 2c) we see that for the largest inner collection angles (greater than 80mrad, often called high-angle ADF or HAADF)

the scattering cross section drops off monotonically with sample tilt. At the lower detector angle ranges (such as 35-40mrad) the scattering cross section drops off more slowly, or even begins to increase initially with sample tilt for the smallest angles.

Optimising robustness to sample tilt requires careful experiment design in order to maximise the width of the plateau region for a particular sample. Here we have optimised the inner collection angle for the imaging of single crystal Pt nanoparticles. To optimise the inner detector collection angle we simulated a Pt nanocube of thickness 7 atoms, 1.94nm, viewed down the <110> zone axis at a series of different tilts and detector angles. For single atom sensitivity in atom counting of a typically 15 atom thick nanoparticle our error from tilt needs to be less than 2%. Therefore, the optimum detector angle, of 35mrad, was selected from Figure 2b by extracting the largest possible sample tilt tolerable before this 2% deviation is reached, as shown in Figure 3; the peak in this curve is the optimum detector angle for robustness to sample tilt. The decrease in cross section drops off more quickly with respect to tilt for larger detector collection angles. At the smallest collection angles, the cross section increases but then drops off more quickly afterwards. Additionally, to maintain signal to noise ratio we must stay clear of the bright-field disk to keep the maximum signal to background ratio.

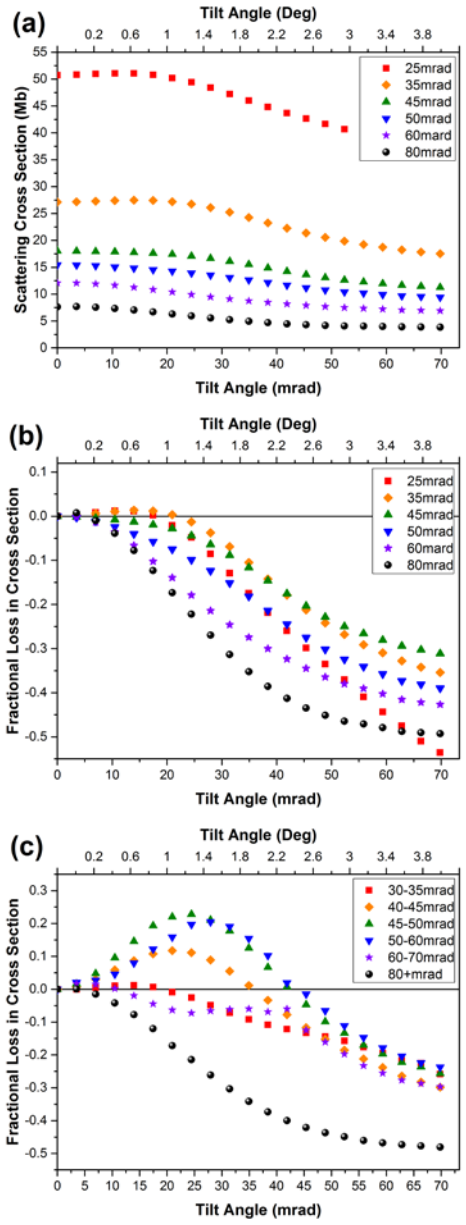

Figure 2 – (a) The dependence of column cross section on sample tilt for a range of detector inner radii with outer radius kept constant at 190mrad. (b) The data presented in (a) now replotted as the fractional change in cross section relative to zero tilt. (c) As for (b) but with narrower annuli of detection to show the detection angle dependence more clearly.

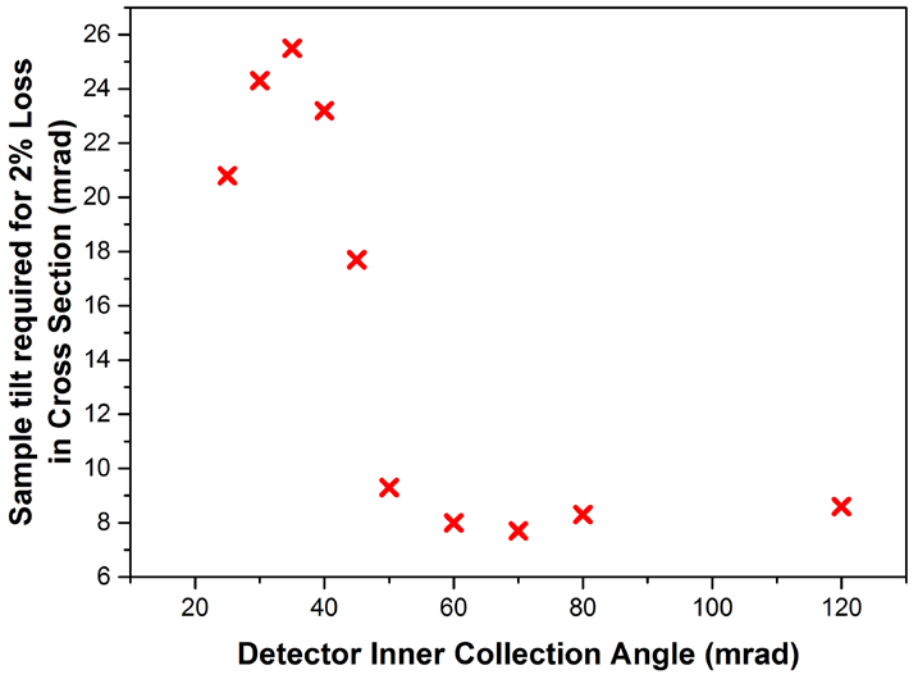

Figure 3 – Graph showing the angle at which angle 2 percent deviation in cross section, from the on axis case, is exceeded for a given detector inner collection angle.

The origin of the plateau at smaller detector collection angles can be investigated theoretically by separating out the elastically and inelastically scattered electron contributions and examining how they contribute to the ADF signal (Figure 4). The elastic signal, initially increases with sample tilt - see Figure 4. The origin of this increase can be explained by understanding the Ewald sphere construction (Figure 5) used to describe Bragg scattering, where scattering occurs most strongly for reciprocal lattice vectors which intersect with the Ewald sphere. For a tilted probe a large number of the higher angle reflections intersect with the Ewald sphere resulting in more scattering out to the detector. In conventional TEM SAD (transmission electron microscopy selected area diffraction) a Laue circle is observed at sample tilts away from a lower order zone axis. We can imagine this Laue circle intersecting the ADF detector when a tilt of half the detector angle, $\beta/2$, is reached resulting in this increase in cross section, see Figure 6. As you push the Laue circle further out for

larger tilts it gets fainter due to the Debye-Waller factor, resulting in a drop off in the elastic contribution to the cross section.

The Ewald sphere construction does not apply to TDS which therefore drops off monotonically with sample tilt, much in the same way as the HAADF images drop off monotonically with tilt. With tilting the atoms are less well aligned resulting in a reduction in the channelling and therefore a lower cross section. At sufficiently large detector collection angles the signal can be assumed to be entirely TDS [11], and therefore the similarity to the tilt curves for large detector collection angles is expected.

There is therefore a detector inner angle for the initial increase in the elastic signal with sample tilt that almost perfectly compensates for the TDS; with the overall result of producing a tilt robust region where the cross section hardly varies. At larger sample mis-tilts, beyond 20mrad in this case, the cross section drops off rapidly trending towards the value predicted by a simple linearity assumption i.e. where a 7 atom thick crystal has the same cross section as 7 times one atom. Whilst it would be ideal to work in this linear regime; it comes at a cost of both resolution and a large tilt dependence variation in the cross section.

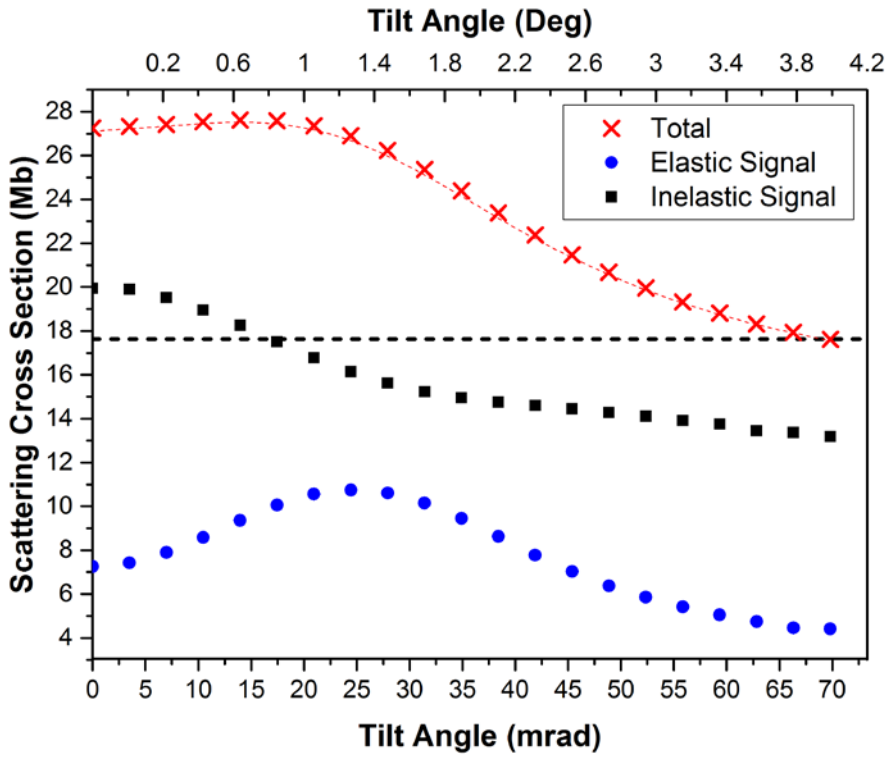

Figure 4 - Graph shows the scattering cross section of a 7 atom thick crystal of Pt separated into the elastic and TDS scattering components. At small tilts below the convergence angle of 20.2mrad there is a plateau region in the total cross section, where it is remarkably robust to tilt, due to balance between the elastic and TDS contributions to the signal. Towards large tilts we see the complete loss in channelling as the cross section value trends towards the linear model, dotted black line.

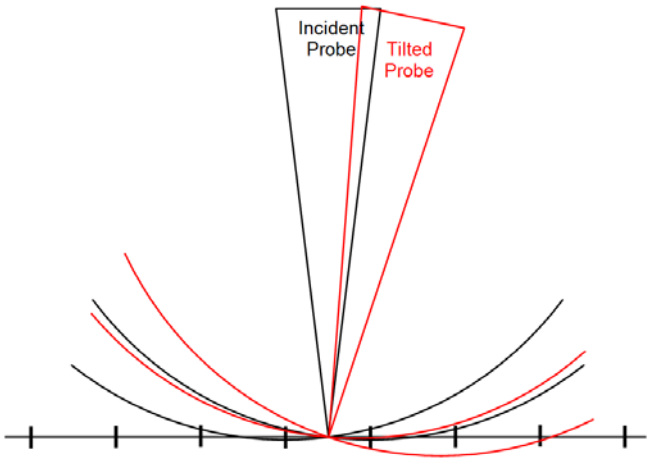

Figure 5 – Diagram of the Ewald Sphere construction for both and on axis, black and a tilted probe, red. Due to the convergence of the STEM probe the Ewald construction is blurred out over a small range of angles. The tilted probe intersects with reciprocal lattice spots (represented by short vertical lines) corresponding to higher scattering angles than the on-axis beam.

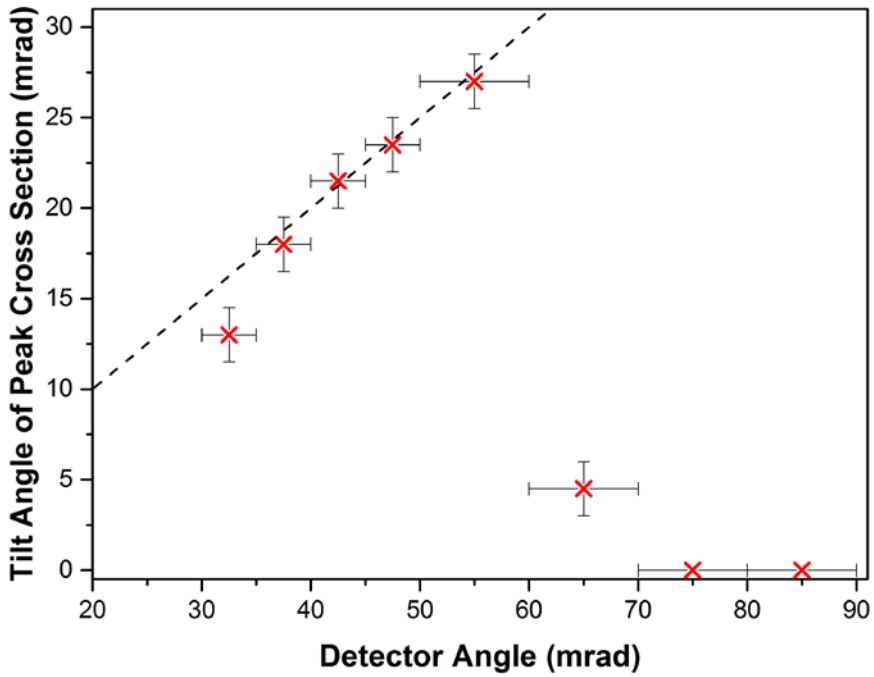

Figure 6 – Graph showing the location of the peak in cross section with tilt for given detector collection inner angles. The peak increases with collection angle due to the intersection of the Ewald sphere with more reciprocal lattice points. It drops off at larger inner collection angles where the angle is sufficiently large that there is no elastic contribution to the cross section.

Another microscope parameter which can be controlled is the probe convergence angle. Figure 7 shows that the plateau region scales with the convergence angle meaning that increasing the probe convergence angle can also be used to extend the plateau region. The convergent electron beam in STEM provides a range of incident angles which results in a broadening to the range of reciprocal points intersected by the Ewald sphere, which provides the convergence angle dependence witnessed in our simulations. For the 28.2mrad convergence angle in Figure 7 the plateau region begins to shrink again preventing further extension of the plateau beyond this point.

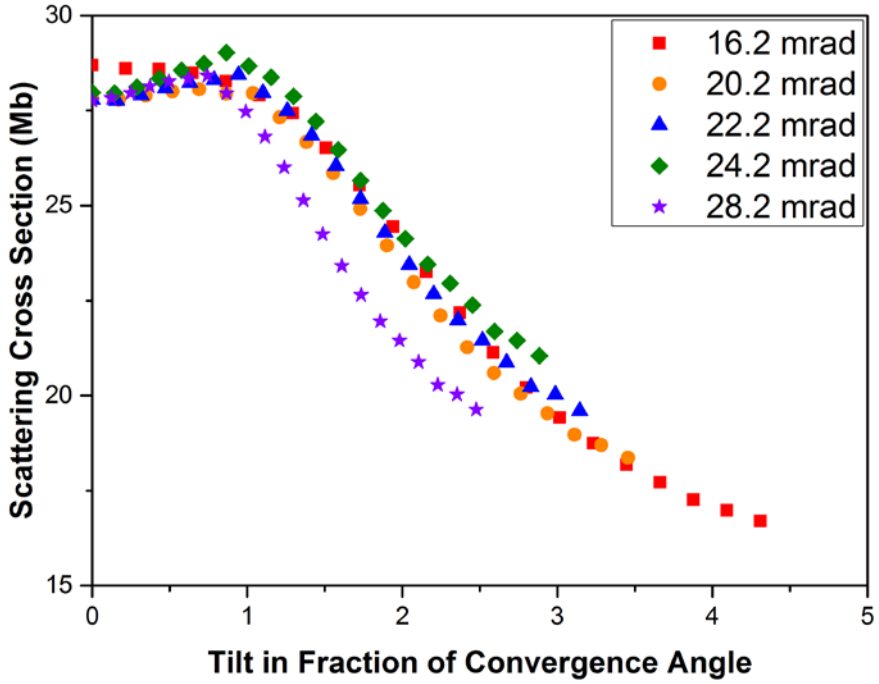

Figure 7 – A normalised graph demonstrating the dependence of the plateau region on the incident probe convergence angle for fixed detector collection angles of 35-190mrad. For each convergence angle the cross section remains roughly constant at small tilts but then drops off quickly after exceeding one convergence angle of tilt.

Focusing only on three different detector collection angles allows us to explore how the decrease in cross section behaves for different sample thicknesses, as shown in Figure 8. It is important to note that the percentage decrease in cross section generally becomes larger in magnitude with increasing sample thickness. This can be explained geometrically as the same sample tilt angle will produce a larger offset between the top and bottom atoms at larger sample thicknesses resulting in a larger decrease in cross section. In order to be able to compensate for the decrease in cross section with tilt by up-scaling the images after acquisition it is necessary for all areas of the image to receive the same scaling. As the plots are in percentage a uniform up-scaling the change in cross section would need to be constant with sample thickness. However single atom thickness will always demonstrate zero decrease in cross section tilt. At larger thicknesses the curves flatten out

which means for thicker samples a post processing method of 'up-weighting' may be possible. Figure 8 demonstrates that a simple up-scaling is not possible therefore we need to optimise experimental conditions for maximum robustness to tilt. The oscillations seen with thickness are due to the oscillation of the electron probe as it is channelling down an atomic column [21]. At a small tilt of 17.5mrad (1˚, within the plateau region) the cross section only oscillates around a mean of zero, for the 35mrad detector, Figure 8a. For the larger detector angles this variation is overlaid a on decrease in the cross section. Even at larger mis-tilts, beyond any plateau region (see Figure 8b), where we have a considerable decrease in the cross section, this seems to be significantly reduced by using the smaller detector collection angle.

The example simulated images in Figure 8 are displayed on a common grey scale, demonstrating the significant increase in counts available for smaller detector angles. The images also show that when a sample is tilted sufficiently such that a decrease in cross section will occur, there is clear ellipticity of the atomic columns visible in the image. Therefore it is obvious to the user at the microscope if an image is unlikely to provide the basis for accurate quantification. Experimentally such ellipticity could be confused with astigmatism however, astigmatism is constant with sample thickness where as tilt is not. For tilted specimens, thicker regions of the sample will appear more elliptical than thinner regions of the specimen. In this way astigmatism and tilt effects could be separated.

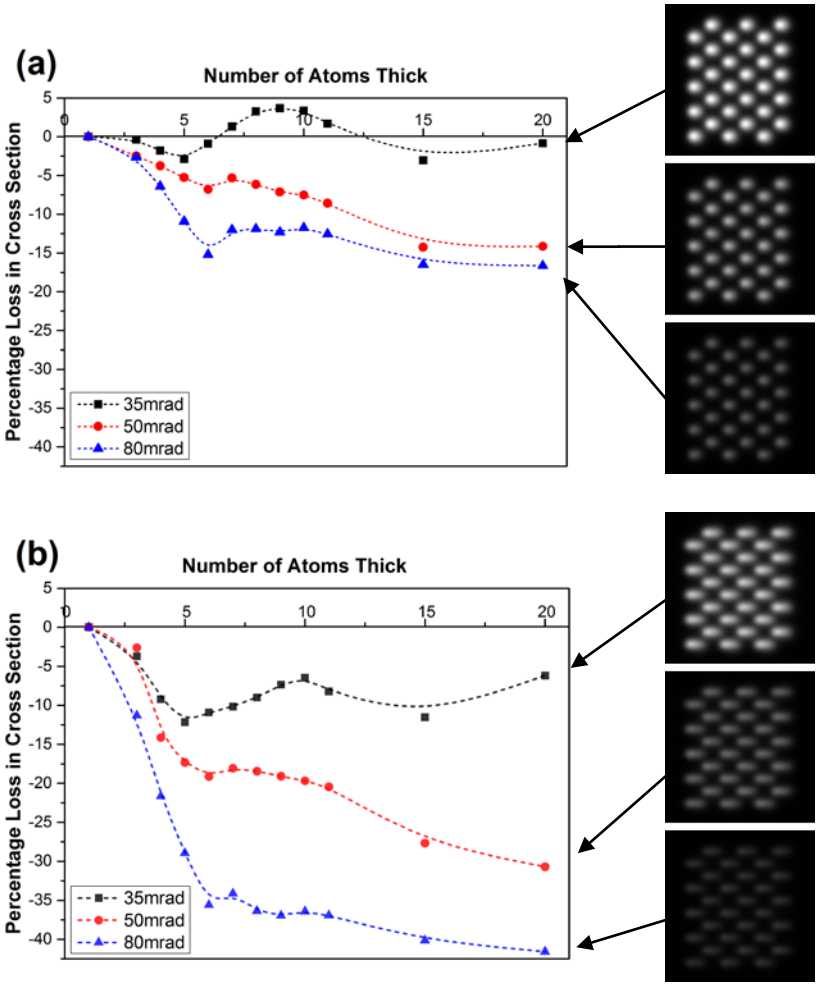

Figure 8 – The graphs shows the percentage decrease in cross section after (a) 1 degree tilt and (b) 2 degree tilt from a 110 viewing direction with increasing number of atoms. Examples of the simulation images from which the cross sections were calculated are displayed to the right of the graphs for 20 atoms thickness, present on the same grey scale.

4 – Bimetallic Systems

The ratio between elastic and TDS scattering changes for different elements. Therefore the conditions optimised to produce a plateau for one element may be less optimal for other elements, Figure 9(a). For lighter elements, like the nickel in Figure 9(b), we see a larger fraction of elastic signal or smaller relative fraction of the TDS signal. This will result in the optimised detector collection angle for tilt robustness being larger than the 35mrad angle for Pt. The similarity between the Pd and Pt curves, Figure 9(a), demonstrates that, provided there isn't larger variation

than 40 in atomic number within one sample it will be possible to optimise the tilt robustness to the average atomic number of the sample.

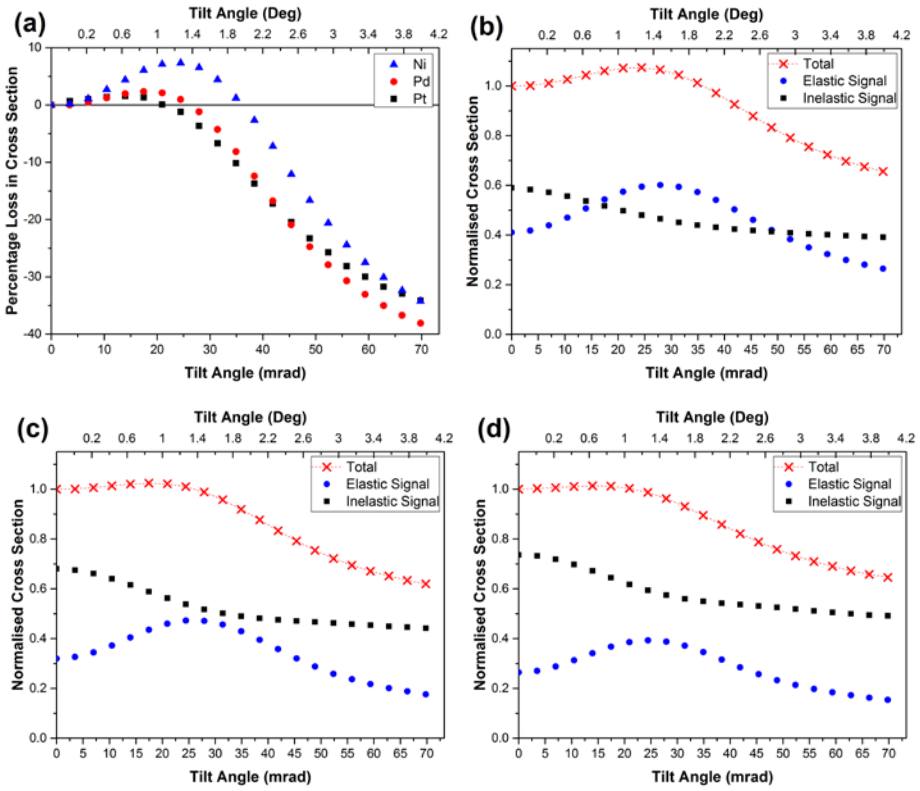

Figure 9 –Graph (a) demonstrates the effect of element on the tilt independent plateau for a fixed detector inner angle of 35mrad. Fractional change in cross section for Ni (b), Pd (c), and Pt (d) has been separated into the elastic and TDS components.

Finally we investigate the effect of bimetallic columns. We know from channelling theory that the location of a secondary atom in an atomic column affects how much it contributes to the cross section. This is often referred to as a Top-Bottom effect, see Figure 10. When tilting away from a crystal zone axis, because we lose that channelling contribution to the cross section, the two atomic columns with the same composition and thickness but different ordering move much closer together in cross section value. At large tilts, where channelling is largely eliminated, ordering within an atomic column no longer affects its cross section value.

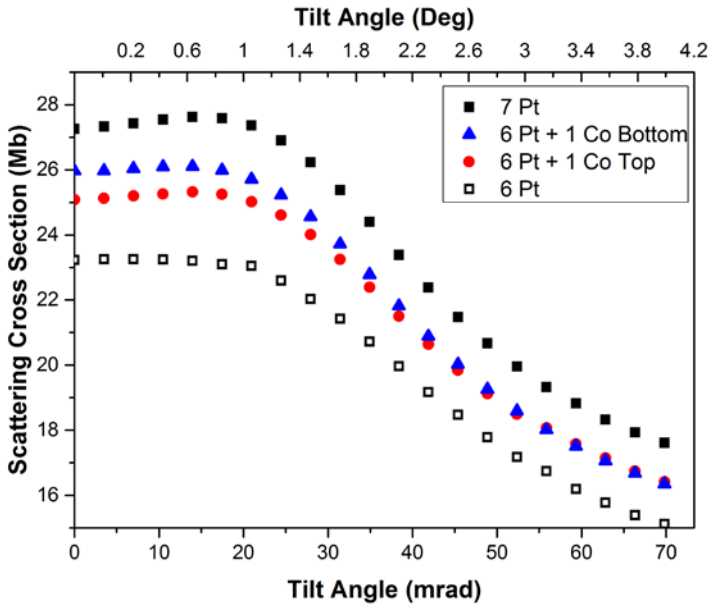

Figure 10 – Graph demonstrates the loss of top-bottom effect when tilting away from a 110 zone axis of a 7 atom Pt crystal, with the top, red, or bottom, blue, atoms replaced with an atom of Co. The red and blue points demonstrate the top-bottom effect due to channelling when the crystal is on axis, but this separation reduces with increasing tilt. The tilt curve for a 6 atom thick Pt crystals is included to give an idea of scale for this effect.

5 – Conclusions

Channelling contributions to the scattering cross section of an atomic column provide additional intensity when the sample is on axis but decreases with sample tilt as the atoms become less well aligned to the incident beam direction. This can cause an error in quantitative measurements; particularly with beam sensitive samples where it is difficult acquire an on axis image. The decrease in the scattering cross section at a given tilt does not scale uniformly with thickness making it impossible to compensate with a scaling factor across an image. We therefore recommend experiment design to minimise this error.

The dependence of cross section on sample mis-tilt can be diminished using a smaller detector collection angle, at least in the case studied here of very thin specimens. This is due to the balance

between elastic and TDS contributions to the signal. The TDS signal drops off smoothly with tilt whereas the elastic signal initially increases with tilt due to the intersection with the Ewald sphere in reciprocal space. At smaller detector angles there is both a larger elastic contribution at smaller collection angles and a larger total scattered intensity which will provide signal to noise gains, assuming Poisson noise which follows a $\sqrt{N}$ relationship (where N is the raw intensity counts in an image). A larger probe convergence angle can also be use to increase the width of the mostly tilt independent plateau as this broadens the Ewald sphere construction. With careful simulations it is possible to design a sample-specific set of experiment design guidelines to maximise this effect, whilst also gaining improvement in counts and therefore signal per unit dose on the sample. Care should be taken for using low angles if there is significant strain present as this could produce artefacts. However in the case where tilt is the limiting factor on quantification accuracy this approach should be used.

This investigation has been carried out only looking at platinum; however we also know atomic number affects the degree of lensing which the atoms provide. Figure 9 shows that and inner angle optimised for Pt does not produce a plateau for lighter metallic crystals. However, we believe we have demonstrated the general framework to understand the channelling nature for simple crystal structure materials in order to obtain a sample-specific set of experiment design guidelines.

6 – Acknowledgments

K.E. MacArthur gratefully acknowledges the EPSRC for PhD funding and Johnson-Matthey for both financial support and scientific guidance and discussions that provided the incentive for this investigation. The authors would also like to acknowledge S Van Aert, A De Backer and G Martinez

for their useful discussions towards investigating this area. The research leading to these results has received funding from the European Union Seventh Framework Programme under Grant Agreement 312483 - ESTEEM2 (Integrated Infrastructure Initiative–I3). This research was supported under the Australian Research Council's Discovery Projects funding scheme (Projects DP110102228 and DP140102538)and its DECRA funding scheme (Project DE130100739).

7 – References

[1] P.D. Nellist, S.J. Pennycook, Adv. Imaging Electron Physicsand Electron Phys. 113 (2000) 147.

[2] H. Katz-Boon, C.J. Rossouw, C. Dwyer, J. Etheridge, Ultramicroscopy 124 (2013) 61.

[3] J.M. LeBeau, S.D. Findlay, L.J. Allen, S. Stemmer, Nano Lett. 10 (2010) 4405.

[4] S.I. Molina, M.P. Guerrero, P.L. Galindo, D.L. Sales, M. Varela, S.J. Pennycook, J. Electron Microsc. (Tokyo). 60 (2011) 29.

[5] S. Van Aert, J. Verbeeck, R. Erni, S. Bals, M. Luysberg, D. Van Dyck, G. Van Tendeloo, Ultramicroscopy 109 (2009) 1236.

[6] L. Jones, K.E. MacArthur, V.T. Fauske, A.T.J. van Helvoort, P.D. Nellist, Nano Lett. 14 (2014) 6336.

[7] R. Ishikawa, A.R. Lupini, S.D. Findlay, S.J. Pennycook, Microsc. Microanal. 20 (2014) 99.

[8] A. Singhal, J.C. Yang, J.M. Gibson, Ultramicroscopy 67 (1997) 191.

[9] N.P. Young, Z.Y. Li, Y. Chen, S. Palomba, M. Di Vece, R. Palmer, Phys. Rev. Lett. 101 (2008) 246103.

[10] J.M. Lebeau, S.D. Findlay, L.J. Allen, S. Stemmer, Phys. Rev. Lett. 100 (2008) 206101.

[11] A. Rosenauer, K. Gries, K. Müller, A. Pretorius, M. Schowalter, A. Avramescu, K. Engl, S. Lutgen, Ultramicroscopy 109 (2009) 1171.

[12] S.D. Findlay, J.M. Lebeau, Ultramicroscopy 124 (2013) 52.

[13] A. Rosenauer, K. Gries, K. Müller, M. Schowalter, A. Pretorius, A. Avramescu, K. Engl, S. Lutgen, J. Phys. Conf. Ser. 209 (2010) 012009.

[14] S. Van Aert, A. De Backer, G.T. Martinez, B. Goris, S. Bals, G. Van Tendeloo, A. Rosenauer, Phys. Rev. B 87 (2013) 064107.

[15] S. Van Aert, K.J. Batenburg, M.D. Rossell, R. Erni, G. Van Tendeloo, Nature 470 (2011) 374.

[16] A. De Backer, G.T. Martinez, A. Rosenauer, S. Van Aert, Ultramicroscopy 134 (2013) 23.

[17] C. Dwyer, C. Maunders, C.L. Zheng, M. Weyland, P.C. Tiemeijer, J. Etheridge, Appl. Phys. Lett. 100 (2012) 191915.

[18] M. Retsky, Optik (Stuttg). 41 (1974) 127.

[19] H. E, K.E. MacArthur, T.J. Pennycook, E. Okunishi, A.J. D'Alfonso, N.R. Lugg, L.J. Allen, P.D. Nellist, Ultramicroscopy 133 (2013) 109.

[20] S. Maccagnano-Zacher, K.A. Mkhoyan, E.J. Kirkland, J. Silcox, Ultramicroscopy 108 (2008) 718.

[21] D. Van Dyck, M. Op de Beeck, Ultramicroscopy 64 (1996) 99.

[22] E. Rotunno, M. Albrecht, T. Markurt, T. Remmele, V. Grillo, Ultramicroscopy 146 (2014) 62.

[23] R.F. Loane, E.J. Kirkland, J. Silcox, Acta Crystallogr. Sect. A Found. Crystallogr. 44 (1988) 912.

[24] P.M. Voyles, D.A. Muller, E.J. Kirkland, Microsc. Microanal. 10 (2004) 291.

[25] P.M. Voyles, J.L. Grazul, D.A. Muller, Ultramicroscopy 96 (2003) 251.

[26] J. Hwang, J.Y. Zhang, A.J. D'Alfonso, L.J. Allen, S. Stemmer, Phys. Rev. Lett. 111 (2013) 266101.

[27] R. Ishikawa, A.R. Lupini, S.D. Findlay, T. Taniguchi, S.J. Pennycook, Nano Lett. 14 (2014) 1903.

[28] A. De Backer, G.T. Martinez, K.E. MacArthur, L. Jones, A. Béché, P.D. Nellist, S. Van Aert, Ultramicroscopy 151 (2015) 56.

[29] A. De Backer, A. De wael, J. Gonnissen, S. Van Aert, Ultramicroscopy 151 (2015) 46.

[30] B.D. Forbes, A. V. Martin, S.D. Findlay, A.J. D'Alfonso, L.J. Allen, Phys. Rev. B 82 (2010) 104103.

[31] (n.d.).

[32] H.X. Gao, L.-M. Peng, Acta Crystallogr. Sect. A Found. Crystallogr. 55 (1999) 926.

[33] D.O. Klenov, S.D. Findlay, L.J. Allen, S. Stemmer, Phys. Rev. B 76 (2007) 014111.

[34] R.F. Egerton, Ultramicroscopy 145 (2014) 85.

[35] Z. Yu, D.A. Muller, J. Silcox, J. Appl. Phys. 95 (2004) 3362.